Chemical Engineering Journal 450 (2022) 138402

Contents lists available at ScienceDirect

Chemical Engineering Journal

journal homepage: www.elsevier.com/locate/cej

Insights into *in-situ* catalytic degradation of plastic wastes over zeolite-based catalyst from perspective of three-dimensional pore structure evolution

Dan Xu [a,b], Xuekun Lu [b], Yeshui Zhang [b,c,*], Paul R. Shearing [b], Shuping Zhang [d,*], Dan J.L. Brett [b], Shurong Wang [a,*]

[a] State Key Laboratory of Clean Energy Utilization, Zhejiang University, Hangzhou 310027, China
[b] Electrochemical Innovation Lab (EIL), Department of Chemical Engineering, University College London, Torrington Place, London WC1E 7JE, UK
[c] School of Engineering, University of Aberdeen, Aberdeen AB24 3UE, UK
[d] School of Energy and Power Engineering, Nanjing University of Science and Technology, Nanjing 210094, China

ARTICLE INFO

Keywords:
Plastic wastes
Catalytic degradation
Zeolite catalyst
Structural evolution

ABSTRACT

Insightfully understanding the process of volatiles from plastic depolymerization entering from the exterior into internal structure of catalyst favors to rationalize the catalyst design in scale-up principles. Herein, catalytic degradation of plastic wastes with fluid catalytic cracking catalyst (FCC) was investigated in-depth. The yield and composition of liquid and gas products over various FCCs were studied quantitatively. The structural evolution of catalyst on overall scope, including the topology of heterogeneous pore systems and spatial distribution of zeolite was probed by X-ray nano-CT. The results showed that FCC enhanced the transformation of C_{16}-C_{30} chains to C_9-centered monocyclic aromatics. The nano-CT analysis of FCCs illustrated remarkable loss of exterior porosity after reaction, particularly at the depth of ~16.5μ m from the outmost layer. While the interior pores were marginally affected, indicating large hydrocarbons incapable of engaging with active sites to full advantage, which preferably occupied large-size pores (>385 nm) of external surface.

1. Introduction

Plastic polymers are irreplaceable in the global economy, with myriad uses in packaging, construction, transportation, electronics and health-care industries. The overall recycling rate of global plastic wastes dominated by mechanical approach is only 16 % in 2018, while 66 % of them is estimated to be landfilled or disposed to the environment [1], rendering a global waste catastrophe, with widespread environmental, economic and health-related consequences. Additionally, since the overwhelming breakout of COVID-19, the great demand of single-use synthetic polymers (e.g. facial masks and protective suits) also aggravated the recycling difficulty of plastic wastes due to its highly biohazardous propensity and complexity in sorting process. Chemical recycling enables circular generation of value-added products far beyond the scope of mechanical recycling, albeit being more energy intensive [2,3]. Wherein catalytic pyrolysis is a desirable thermochemical means to efficiently degrade plastic wastes into different monomers and chain length into smaller molecules, simultaneously mitigating green-house gas emission [4,5].

Polyolefin wastes, such as polyethylene (PE) and polypropylene (PP) account for 63 % in plastic wastes [6], which exhibit resilient aliphatic C—H and sp^3 C—C bonds that are arduous to cleave. In petroleum refinery industry, the high-molecular-weight hydrocarbons of crude oils can be converted into gasoline, olefinic gases and base chemicals over fluid catalytic cracking (FCC) unit [7–9]. A commercial FCC catalyst normally comprises of crystalline zeolite-Y or faujasite as active sites, amorphous aluminosilicate phase as stable matrix, plus fillers and binders to provide the physical strength and integrity. The microporous zeolite consists of silica and alumina tetrahedral, allowing the transferring and cracking of molecules smaller than C_{12} hydrocarbons owing to its micropore-size (~7.4 Å) confinement [10,11]. The matrix with acidity builds up an interconnected network of micro-, *meso*- and macropores for heavy compounds accessing into internal surface and precracking. Considering the structural similarity of polyolefins-derived tar and crude oil, it is of great prospect to utilize FCC catalyst to transform petroleum-based plastic wastes into aromatics, olefins and

* Corresponding authors at: School of Engineering, University of Aberdeen, Aberdeen AB24 3UE, UK (Y. Zhang).
E-mail addresses: yeshui.zhang@ucl.ac.uk (Y. Zhang), zhangpeyton@163.com (S. Zhang), srwang@zju.edu.cn (S. Wang).

https://doi.org/10.1016/j.cej.2022.138402
Received 10 May 2022; Received in revised form 2 July 2022; Accepted 23 July 2022
Available online 3 August 2022

paraffins in a scale-up application [12–15]. Andreas et al. [16] employed steam-treated FCC catalysts for in-line catalytic upgrading of polyolefin and found the FCC catalyst obtained higher yields of C_5-C_{11} aliphatics up to 42 wt%, that is more active than the HZSM-5-containing additives in converting C_{12+} products. Saeaung et al. [17] performed catalytic pyrolysis of polyolefin plastics investigation on the degradation of FCC catalyst in a continuous process. The results showed that spent FCC reduced the production of waxes with increasing yield of gasoline-range hydrocarbons and aromatics. The author hypothesized that catalytic cracking behavior took place mainly within the pores rather than on the external sites of the catalysts. Vollmer et al. [18] compared fresh and equilibrium FCC catalyst for catalytic cracking of PP. Despite the reduced accessibility and activity in equilibrium FCC, both of the catalysts produced approximate yield of aromatics (~21 %), simultaneously with decreased coke formation in equilibrium FCC. This result was likely ascribed to the deposited metals on the exterior of the equilibrium catalyst restricting mass transport to the interior acid sites to form coke, therefore to enhance cracking activity.

Previous studies have been focused on probing the influencing mechanism of the acidity of zeolite with related microporous structure on the aromatization of petroleum-based plastic wastes [19–22]. Actually, long-chain polymer molecules of heavy hydrocarbons cannot directly enter the acid sites of micropores of the catalyst due to the restricted access and slow migration. Then, thermal pre-cracking on mesoporous and macroporous networks formed by aluminosilicate played an important role in the degradation process and the ultimate product distribution from plastic conversion over FCC catalyst particles [18,23]. Although the open pore structure of zeolite-based catalyst can enhance the accessibility of active site of catalytic reactions, it also lacks the shape-selective of active sites in the micropores. Meanwhile, the larger pore size leads to a higher degree of coke condensation in the catalytic pyrolysis, due to the accumulation of more volatiles caused by the less diffusion resistance [24]. Therefore, the spatial distribution of zeolite with hierarchical porous matrix is of significance to catalytic process. Nevertheless, it is still unclear how primary volatiles from plastic depolymerization enter deeper into internal pore network of catalyst from the exterior architecture intuitively. In addition, the spatial change of pore structure caused by coke formation correlated to catalytic performance still remaining to be revealed. The above-mentioned information is of highly necessity because it favors to rationalize and develop the catalyst design in scale-up principles for better catalytic effects.

In order to insightfully understand catalytic degradation behaviors of plastic wastes over zeolite-based catalyst, the structural evolution of catalysts over the whole range of length scales, as well as the topology of heterogeneous pore systems, and the spatial distribution of the zeolite and matrix need to be investigated in-depth. For this purpose, the objective of work is to instigate a series of FCC catalysts for catalytic degradation of plastic wastes with quantitatively gas and oil products analysis over FCC catalysts. The hierarchically porous architecture before and after reaction in three-dimensional(3D) perspectives together with zeolite distribution were reconstructed by X-ray nano-computed tomography (X-ray CT). Also, characterizations such as N_2 adsorption/desorption, X-ray diffraction (XRD), temperature-programmed desorption of ammonia (NH_3-TPD) and temperature programmed oxidation (TPO) analysis of the used FCC catalyst were carried out to precisely elaborate on the catalyst deactivation mechanism during catalytic cracking process of plastics.

2. Materials and methods

2.1. Materials preparation

PE obtained from In2 Plastic ltd of UK is used as representative of plastic waste, with the particles size of around 2 mm. Two types of spherical FCC catalysts (FCC1 and FCC2) were acquired from riffling large batches, same as previously reported work [25]. The average size of the above-mentioned FCC particles ranges from 60 to 100 μm, with an imperfect spherical shape and the same density of 1420 kg m^{-1}. The proximate and ultimate analysis of the feedstock is listed in Table S1 of Supporting Information. Prior to experiment, the catalyst samples were dried in an oven at 100 °C for 8 h to remove moisture. The elemental composition of the fresh catalysts was measured by X-ray fluorescence spectrometry (XRF).

2.2. Catalytic pyrolysis experiment

The *in-situ* catalytic pyrolysis experiment was performed in a bench-scale fixed-bed system, seen in Fig. 1 [26]. The high-purity nitrogen (≥99.99 %) with a flow rate of 100 mL min^{-1} was purged into reactor (ϕ: 35 mm; L: 300 mm) to ensure air-isolated atmosphere. 1 g of PE was homogeneously mixed with same quantity of FCC1 or FCC2 and subsequently loaded on the perforated plate of ceramic basket. Then it was suspended in the middle of the pyrolysis furnace. The K-type thermocouple was placed in the middle of pyrolysis stage to measure real-time temperatures. The pyrolysis stage started to heat from 25 to 600 °C at a heating rate of 20 °C min^{-1} and hold for 10 min, whilst the reaction time was recorded. The condensable products in evolved volatile were captured by a condensation system, which consisted of an empty condenser cooled by antifreeze mixture, then followed by two coalescence filters to retain aerosol particles larger than 0.1 μm. The non-condensable gas was sampled in 5 L Tedlar gas sampling bags for further characterizations. After cooling down the reactor to room temperature, the FCC catalysts were weighed to preliminarily calculate the amount of carbon deposition. In comparison to catalytic cracking, thermal pyrolysis of PE without catalyst was conducted according to above-mentioned steps. Each run has been carried out at least 3 times to ensure reproducibility of the experiments.

2.3. Characterization and analysis

The composition of gaseous products including H_2 and light hydrocarbons (C_1-C_6) were quantified by a Thermo Scientific Trace 1310 gas chromatograph equipment (GC). The GC was equipped with thermal conductivity detector (TCD) and Flame ionization Detector (FID). TCD was used for the analysis of H_2, CO and CO_2, fitted with 10 feet length by 1/8 in. diameter column. The FID fitted with 50 m × 0.32 mm × 5 μm (Agilent CP-Al_2O_3/KCl) column was applied for the detection of hydrocarbon gases.

The liquid components were subjected to an Agilent 7250 GC/Q-TOF gas chromatograph-mass spectrometer (GC–MS), which was set at 50 °C for 2 min and then increased to 290 °C at the rate of 8 °C min^{-1} and held for 5 min. The temperature of injector was fixed at 280 °C. 1 μ L of the liquid product was injected into the column with helium (He) as the carrier gas at the flow rate of 1.0 mL min^{-1}. The components of products were separated by a HP-5MS capillary column (30 m × 0.25 mm × 0.25μ m) and the split ratio was kept at 1:60. The NIST MS library v2.0. was used to identify the chromatographic peaks.

NH_3-TPD measurement of fresh FCC catalysts was conducted by an AutoChem II system (Micromeritic, USA). The catalysts were pretreated at 550 °C for 1 h under a He stream (30 mL min^{-1}). After cooling down to 100 °C, it was purged with a 30 mL min^{-1} flow rate of NH_3 for 1 h. Subsequently, He was introduced to remove the weakly adsorbed NH_3, followed by heating the sample up to 800 °C with a temperature ramp of 10 °C min^{-1}. The desorbed products were detected by TCD calibrated for NH_3 analysis.

N_2 adsorption–desorption isotherms of the catalysts was determined using micromeritics 3Flex surface characterization analyser. The catalyst was pre-degassed under vacuum for 12 h at 250 °C. The surface area was determined according to the Brunauer-Emmett-Teller (BET) method over a relative pressure range (P/P_0) between 0.05 and 0.35. The total pore volume and pore width were estimated from N_2 desorption curves

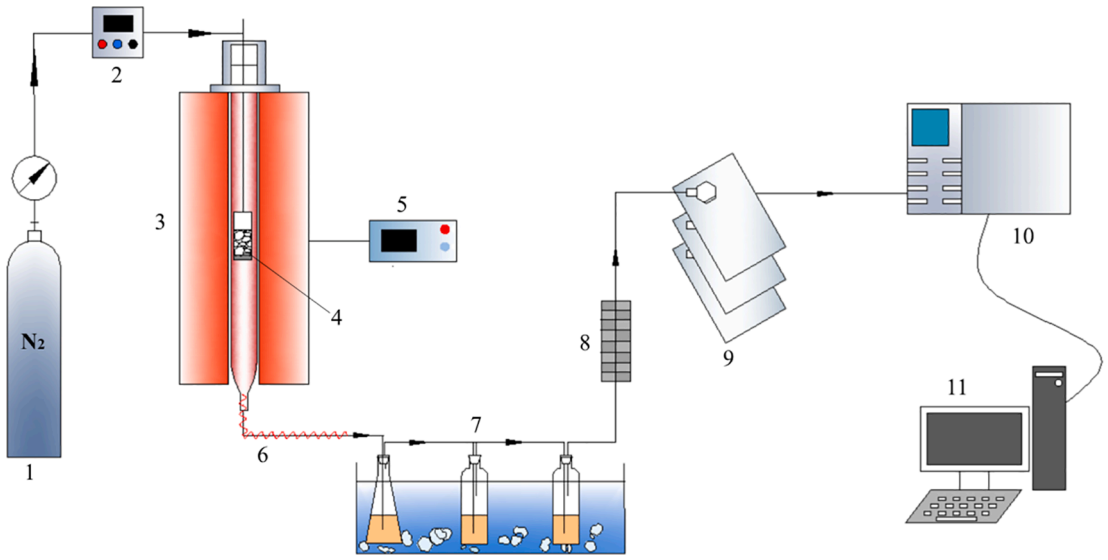

Fig. 1. Schematic diagram of *in-situ* catalytic pyrolysis of plastics over FCC catalysts. 1-nitrogen cylinder; 2-mass flow controller; 3-catalytic pyrolysis reactor; 4-quartz basket with perforated plate; 5- temperature controller; 6-electric heating belt; 7-ice water condensation system; 8-moisture trap; 9-gas bags; 10, 11-gas chromatography.

by the Barette-Jovner-Halenda (BJH) method [27].

The microporous structures of fresh and used catalysts were characterized by a Zeiss Xradia Ultra 810 X-ray microscope (Carl Zeiss, USA), which is a non-destructive technique capable of providing highly resolved quantitative 3D density maps. A single catalyst particle was mounted on a pin using fast-setting epoxy and aligned within the X-ray beam at an isotropic voxel size of ~63 nm and a field of view of 64 μm × 64 μm. A quasi-monochromatic X-ray beam at 5.4 keV from Cr emission characteristic energy was used to collect 1601 sequential projections every 40 s over the full 180° angular rotation with a step size of 0.11°, as displayed in Fig. S1. Two kind of large field-of-view (LFOV) scanning modes were adopted comprehensively. These radiographic projections were corrected by the alignment of center shifts, then reconstructed by a standard filtered back projection algorithm in the Zeiss Scout and Scan software package (Carl Zeiss, CA, USA). Post-processing of the reconstructed CT data was imported into commercial Avizo 9.4 software (Thermo Fisher Scientific, UK) for internal structural characterization. The pore size distribution (PSD) was analyzed using local thickness from open source software (Fiji) [28].

Temperature programmed oxidation (TPO) of deposited carbon on the reacted catalysts was analyzed on a thermogravimetric analyzer (NETZSCH, STA 449F3, Germany). Around 20 mg of the spent catalyst was heated to 800 °C at a heating rate of 15 °C min^{-1} and hold for 10 min with an air flow rate of 100 mL min^{-1}.

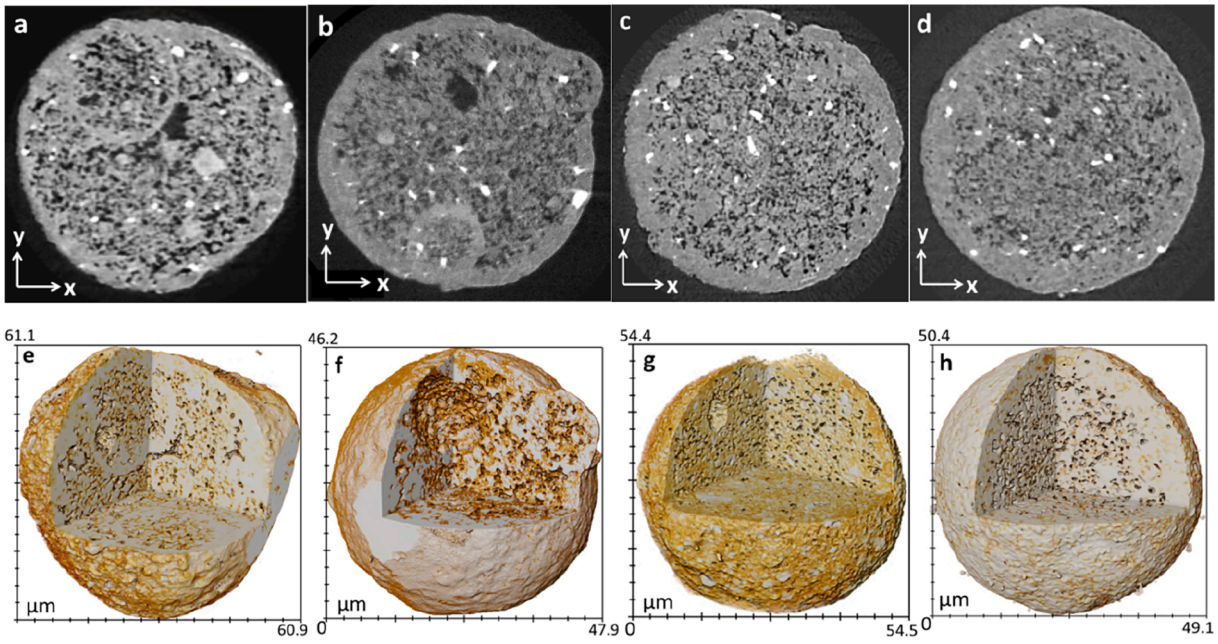

Fig. 2. Microstructure characterization of FCC1 and FCC2 catalysts by X-ray nano-CT. (a-d) Reconstructed images showing one of 1601 virtual orthoslices of fresh FCC1, used FCC1, fresh FCC2 and used FCC2, respectively; (e-h) 3D visualization of the reconstructed fresh FCC1, used FCC1, fresh FCC2 and used FCC2 particles via volume rendering method.

3. Results and discussion

3.1. Characterization of fresh catalysts

The pore structure with acidity distribution in the whole range of catalysts is essential characteristic that can determine the catalytic behavior of PE degradation. Thereby, the spatially structural nature of fresh and used FCC particles is revealed using the highly resolved quantitative 3D density maps from X-ray CT, as seen in Fig. 2. Fig. 2(a-d) show one orthoslicing image of 1601 projections of fresh FCC1, used FCC1, fresh FCC2 and used FCC2 at the voxel size of 63 nm, respectively. Three phases in catalyst particles can be clearly distinguished, which include zeolite (light spots), aluminosilicate matrix and carbon depositions (light grey bulks), as well as connected network of macropores (in dark). It is observed that despite of the presence of zeolite domains in particles, partial of them are embedded in Si-Al skeleton instead of exposing on the surface of catalyst, which could render active sites inaccessible to reactants, thus undermining catalytic performance. The reconstructed 3D structure of FCC catalysts for each particle was conducted with a corner-cut-off using volume rendering method to expose internal structure. As shown in Fig. 2(e-h), the internal structures of FCC catalysts prior to further processing took on indiscernible internal components. These objectives will be subjected to subsequent segmentation and further analysis to reveal the radial structural distribution of pore and zeolite embedded in the catalyst.

The NH_3-TPD profiles and quantification of the total acidity are shown in Fig. 3(a). Both monoliths presented two distinct peaks centered at 120 and 384 °C, indicating the majority of weak acidic sites but low concentrations of strong acidic sites. The total acid quantity of FCC1 (7.2 mmol g^{-1}) is almost the same as that of FCC2 (6.8 mmol g^{-1}), wherein the weak acidity of FCC2 is slightly higher than that of FCC1. The XRF analysis of the chemical composition of fresh catalysts is listed in Table S2. The silicon and alumina oxides made up the major components of FCC catalysts. It reveals similar SiO_2/Al_2O_3 ratio of FCC1 and FCC2 with 2.17 and 2.16, respectively.

The microporous structure of catalysts is studied by N_2 adsorption/desorption isotherm, seen in Fig. 3(b). The porosity parameters of FCC catalysts are summarized in Table 1. The fresh FCC catalysts delivered a combination of type I and IV isotherms according to the IUPAC classification [29]. A characteristic step-down in the desorption branch associated with H4 hysteresis loops are generally observed, indicative of both micro- and mesopores [30,31]. There was a little limitation in adsorption at high P/P_0, which may be caused by the existence of non-rigid aggregates of plate-like particles or assemblages of slit-shaped pores [32]. The specific surface area of pristine FCC1 and FCC2 is 143.0 and 219.7 cm^3 g^{-1}, respectively. While FCC2 took on higher micro-porosity than that of FCC1. After catalytic degradation, the amount of N_2 adsorption decreased remarkably at low P/P_0, demonstrating a remarkable porosity loss. The surface areas of spent FCC catalysts exhibited significant decrement, with FCC1 and FCC2 decreasing to 23.7 and 20.7 cm^2 g^{-1}, accompanied with pore volume declining to 0.05 and 0.04 cm^3 g^{-1}, accordingly. The microporous volume was almost zero due to pore structural collapse and coke formation.

Table 1
The microstructural properties of FCC catalysts.

Sample	S_{BET} (cm^2 g^{-1})	V_T (cm^3 g^{-1})	S_{Micro} (cm^2 g^{-1})	V_{Micro} (cm^3 g^{-1})
Fresh FCC1	143.0	0.11	85.2	0.052
Fresh FCC2	219.7	0.17	115.6	0.067
Used FCC1	23.7	0.05	2.8	0.001
Used FCC2	20.9	0.043	2.5	0.001

3.2. Products analysis

Fig. 4 displays the mass balance of gas, liquid and coke yields of PE degradation with no, FCC1 and FCC2 catalysts. The oil products accounted for the main fraction (64 %) of PE feedstock with no catalyst, wherein the wax-like products were the primary component in oil products. The waxes products normally consist of long-chain

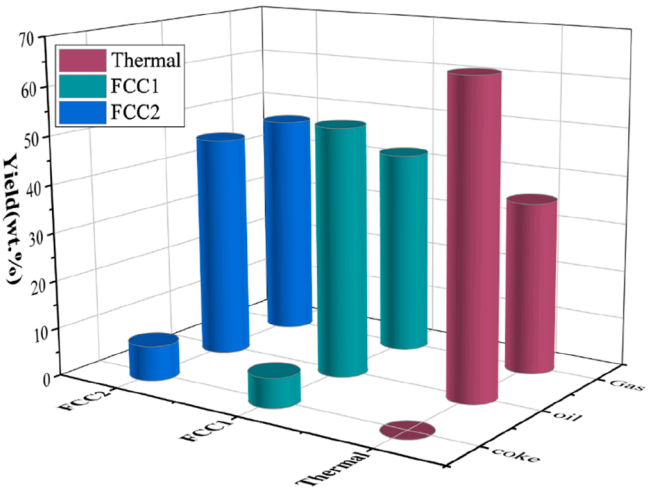

Fig. 4. The gas, liquid and coke yield of PE degradation with no, FCC1 and FCC2 catalysts.

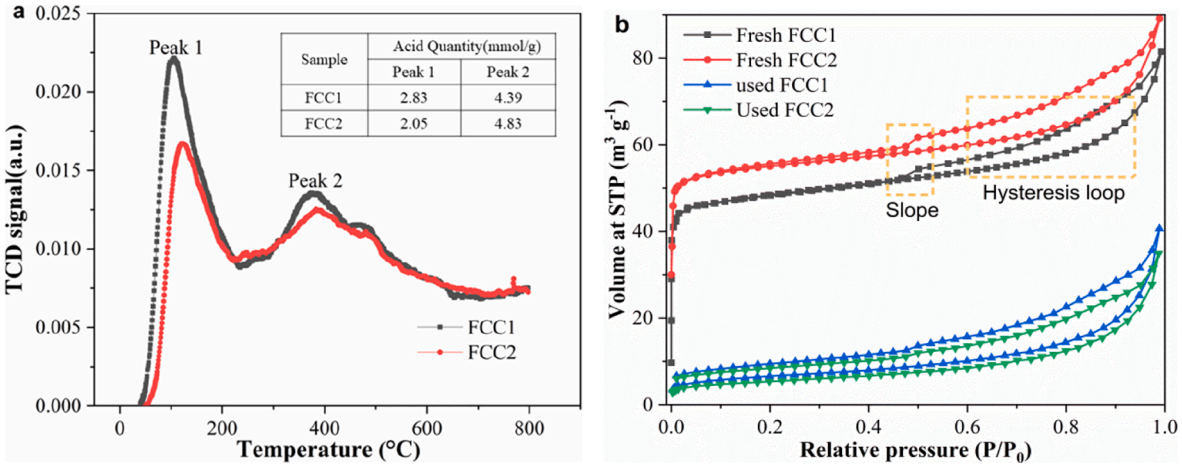

Fig. 3. (a) NH_3-TPD profiles (the table in figure listing the acid quantity of FCC catalysts); (b) N_2 adsorption/desorption isotherm of fresh and used catalysts.

hydrocarbons (linear or branched) heavier than C_{19} [11,16]. With the incorporation of FCC catalysts to PE, the oil yield reduced to 51.6 % for FCC1 and 46.7 % for FCC2 respectively, with wax-like oil being negligible. In comparison to FCC1, FCC2 achieved relatively lower liquid but higher gas product. The phenomenon can be interpreted by the higher porosity of FCC2 that allowed more long chains to access and promoted the cleavage potential such as cracking mechanism to gas products. Consequently, a gas yield of 51.6 % could be obtained for FCC2, which is marginally higher than the gas yield of 46.1 % for FCC1. The result indicated that besides the surface acidity, porous structure also plays an important role in promoting the formation of the hydrogenation steps to synthesis free radicals that enhanced β-scission for the gas production [33]. In general, the incorporation of FCC catalysts favors the cracking of the nascent volatiles to lighter molecules, thus leading to an increase in the formation of gas fraction at the expense of oil components.

The volumetric concentration of gas components from catalytic degradation of PE over FCC is depicted in Fig. 5. For thermal cracking, the gas fraction was mainly composed of butane-predominated C_4 hydrocarbons (~60.48 %). Adding FCC1 and FCC2 to the reaction increased the concentration of lighter C_1-C_3 hydrocarbons from 27.61 to 38.34 % and 72.18 % respectively due to the remarkable activity of FCC for C—C bond scission in ploymers [34]. In comparison to FCC1, FCC2 possessed higher selectivity of light hydrocarbon gas, such as methane, ethane and ethylene. Although there was no great difference between the acidity of these two catalysts, the variety of spatial composition distribution (including zeolite, matrix and porosity) may also result in various gaseous results, as shown in Fig. 10. FCC2 had a higher microporosity and acidity that promote the cracking ability of catalyst. Specifically, part of thermally degraded products (mainly heavy oil fraction from plastic pyrolysis) could more easily access to the acid sites into the catalysts porous structure, leading to higher cracking rate and then generating light volatiles [35]. The light vapors then underwent series reactions such as dehydrogenation and were cracked to form H_2, CH_4, C_2-C_3 alkanes and alkenes. That phenomenon has also been reported by other authors [35–37].

The oil components from catalytic degradation of PE over FCC are elaborated on using gas chromatograph-mass spectrometer, shown in Fig. 6. The GC–MS spectrum of oil from thermal deconstruction of PE showed a series of linear non-branched olefins, *n*-paraffins and wax, with undetectable quantity of aromatics. After the incorporation of FCC catalysts to plastic, numerous characteristic peaks representing monocyclic aromatics emerged. The finding suggested that long-chain polymers have been effectively cracked into light gas and aromatics by undergoing a series reaction of double-bond cleavage and further propagation steps within the zeolite micropores [12]. In addition, a small number of peaks assigned to chain alkane, olefins and

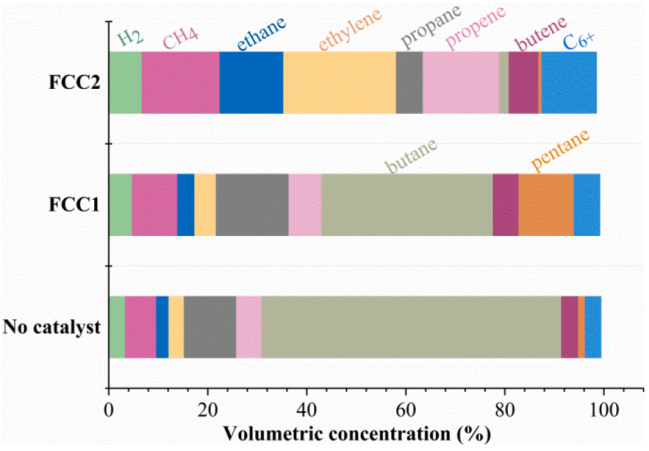

Fig. 5. The volumetric concentration of gas components from catalytic degradation.

cycloalkanes were detected in oil compounds from the cracking process of PE with FCC catalyst, and the abundance of those were weaker than that of aromatics. The similar compositions in liquid oil were formed with the two FCC catalysts. These results proved that FCC catalysts exhibited impressive aromatization activity for the production of light hydrocarbon liquids.

The molecular species in oil are grouped according to their carbon numbers, and the concentrations are expressed in Fig. 7. The carbon numbers derived from thermal cracking delivered a bell-like distribution centered at the C_{17}-C_{22} numbered chains, indicative of a low conversion efficiency of large paraffins and lubricant-range hydrocarbons during the initial thermal cracking steps [22]. In contrast, catalytic degradation of PE over FCC catalysts gave a rise to quantitative degradation of high molecular mass (C_{16}-C_{30}) into a narrow C_9-centered distribution of monocyclic aromatic species. The above-mentioned oil products are abundant of toluene, p-Xylene and various methylbenzenes, which are of greatly commercial interest. In addition, a flattened and low-level distribution of species with carbon numbers from C_{15} to C_{26} appeared over FCC1 and FCC2. Consequently, there is no significant variation in oil components when using both FCC1 and FCC2. FCC2 exhibited a higher content (34.71 %) of monocyclic aromatics than that (25.14 %) of FCC1, wherein C_8 and C_9 were preferable components. Overall, FCC2 exerted higher selectivity of gas hydrocarbons (C_1-C_4), as well as gasoline hydrocarbon fraction (C_5-C_9) than FCC1. The discrepancy in liquid and gas compositions could be contributed by the essentially different structure of FCC catalysts including pore and zeolite distribution in spatial orientation [38].

3.3. *Three-dimensional characteristics of catalyst structure*

Fig. 8 depicts TPO analysis of coke depositions on FCC catalysts from catalytic degradation of PE. It is shown that spent FCC1 and FCC2 contained the deposited coke amount of 5.5 wt% and 6.9 wt% accordingly. The catalyst coke is universally identified as polyaromatic or high-molecular-weight polyaliphatics, which would polymerize on the active sites and hinder pore channels, eventually deactivating the catalysts [26,39]. The structure of FCC catalysts associated with zeolite and pore distribution are tightly correlated to the catalytic activity during PE degradation. Nevertheless, the TPO and BET cannot provide location-specific structure evolution within the FCC catalyst particles. The above techniques are essentially blind to the internal textural properties giving rise to different catalytic performances. That information matters the how volatiles derived from PE decomposition gradually access into the internal structure of catalyst and ultimately sealed off the surficial active sites and pore channels, which can guide the design of catalyst structure for an improved catalytic performance.

In order to cumulatively understand the catalytic degradation process of PE over FCC catalysts, this piece of work is aiming to visualize the microstructure within the hierarchical FCC matrix to fully grasp the different natures of catalyst by X-ray nano-CT. The segmented tomograms of catalysts can be used to estimate the fraction of volumetric composition of each sample, which is shown in Fig. 9. The segmented pore phase is highlighted in pink, zeolite in green, aluminosilicate matrix and coke deposition(ACD) in black by analogy. Fig. 10 demonstrates the radial distribution of three elementary constituents as a function of the distance from the particle center. As observed in Fig. 10(a-b), the zeolite distribution in both fresh FCC1 and FCC2 catalyst delivered a relatively homogeneous tendency alongside the radial orientation of catalyst. The pore composition from the core to the outermost layer of FCC1 fluctuated around 16 %, which was lower than 23 % of FCC2. Combined with BET analysis, FCC2 delivered a more porous structure than FCC1. The aluminosilicate matrix accounted for dominant proportion in fresh catalyst. It is noted that there are several humps appearing between composition curves of aluminosilicate matrix and pore phase, which might be ascribed to macroscopic holes in matrix, thus causing defective structure. This can also be observed from

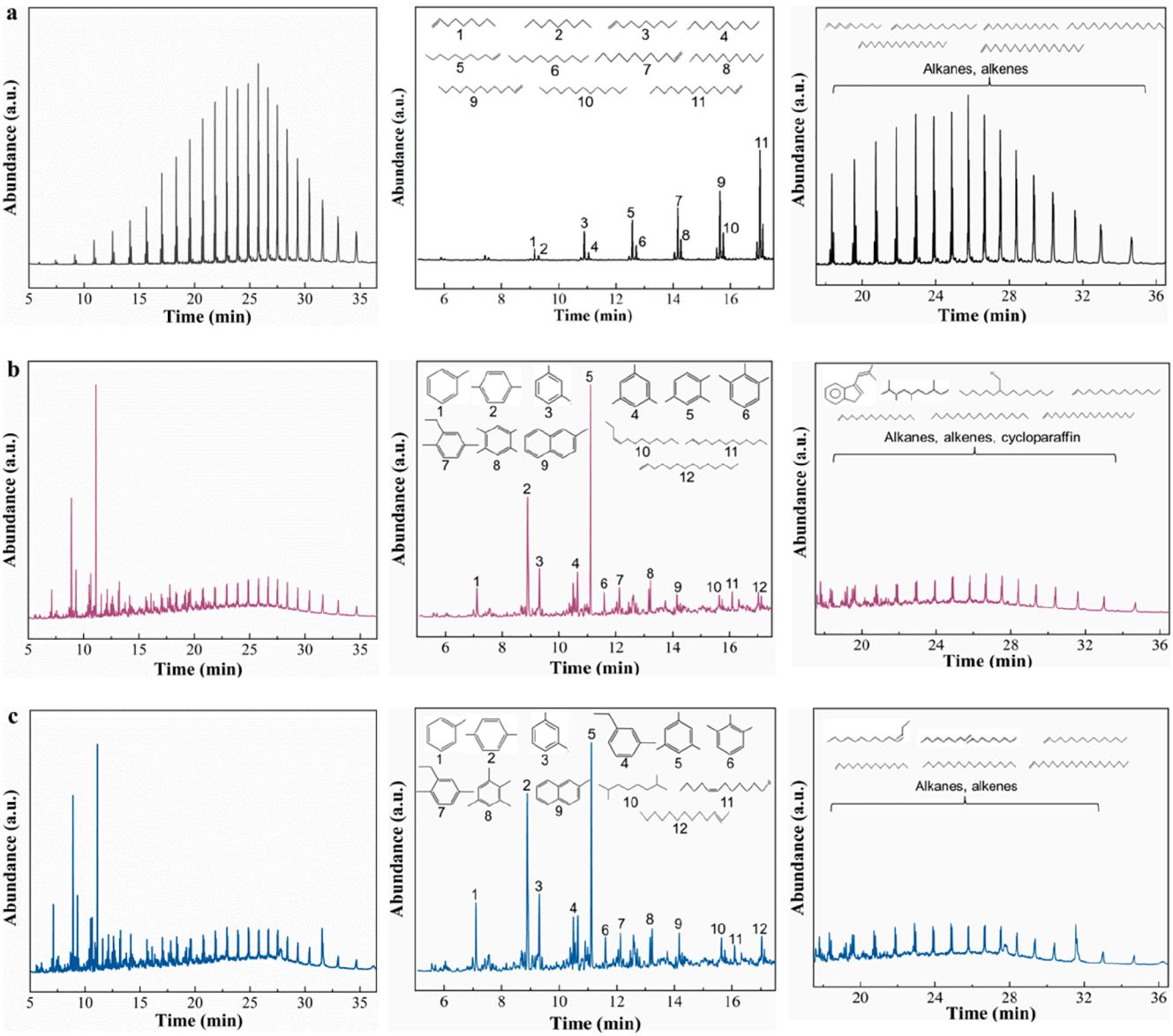

Fig. 6. GC–MS analysis of oil products from degradation of PE under various conditions. (a) raw oil of PE thermal pyrolysis; (b) upgrading oil products over FCC1; (c) upgrading oil products over FCC2. The overall GC–MS patterns and two enlarged regions are shown.

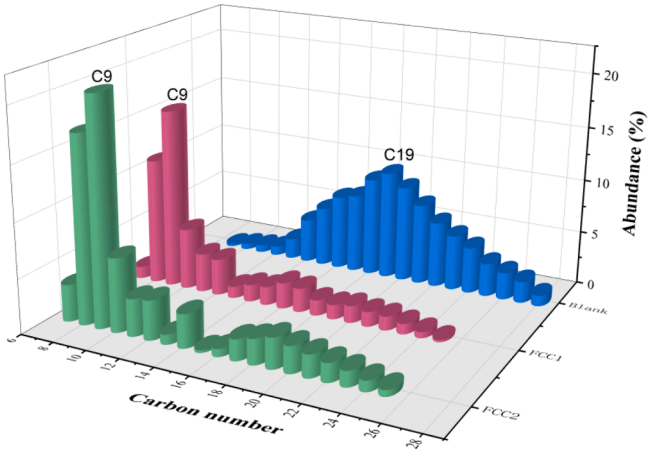

Fig. 7. Products distribution of liquid products obtained from catalytic degradation of PE without catalyst, with FCC1 and FCC2 catalyst.

orthoslicing images from X-ray CT in Fig. 2.

Compared to the fresh counterparts, both spent FCC1 and FCC2 exhibited a declined pore fraction throughout the radial orientation of particles, as seen in Fig. 10(c-d). This attenuation of porous structure could be resulted from coke deposition blocking pore cavities. The TPO analysis can confirm this conclusion. Compared to TPO and BET analysis, this CT-based method can provide a location-specific analysis of coke within the catalyst particles. Specifically, with the increasing distance from the particle center to the exterior of the catalyst, the pore fraction exhibited a downward distribution, gradually approaching zero at the outermost shell. The phenomenon intuitively illustrated a serious loss in exterior pores rather than internal location. The interior porosity of the catalyst is not significantly affected during catalytic cracking process, confirming that PE-derived volatiles were incapable of engaging with active sites to full advantage. This finding is in line with the report carried out by Krumeich [40]. Furthermore, it can be found that the largest loss of pore fraction occurred at the depth of approximately 16.5μ m from the outer surface of particle. It is speculated that despite the pore structure and acid activity in the core location may be retained during catalytic reaction, these surface pore networks

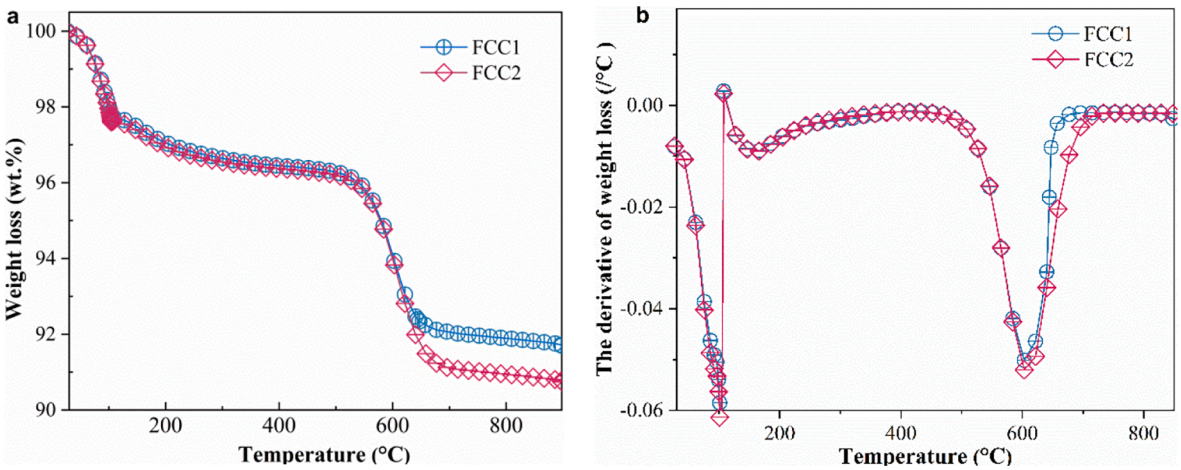

Fig. 8. TPO analysis of coke depositions on FCC catalysts from catalytic degradation of PE.

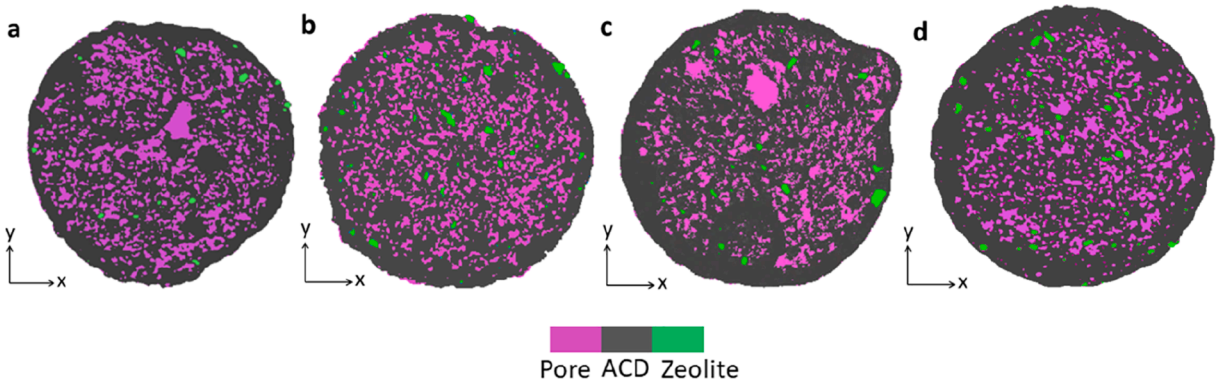

Fig. 9. Segmented tomograms of catalysts: (a) fresh FCC1, (b) fresh FCC2, (c) used FCC1 and (d) used FCC2 (Pore was denoted in pink, ACD in Black and zeolite in green). (For interpretation of the references to color in this figure legend, the reader is referred to the web version of this article.)

ultimately determine the catalytic performance of zeolite domains within the FCC.

Physical gas adsorption is often the first-preference technique to probe hierarchically porous structure ranging from 0.5 to 150 nm [41,42]. Fig. 11 displays the pore size distribution (PSD) of all FCC catalysts, calculated by BJH model from N_2 adsorption/desorption. As shown in Fig. 11, there are two peaks at 4 nm and 10 nm in the volume distribution curves. In previous literatures, the peak at 4 nm is frequently observed and attributed to the presence of real pores [43,44]. Actually, the peak value cannot accurately reflect the exact porous properties of the materials due to the interference of tensile strength effect (TSE) [45,46]. Furthermore, it is discerned that a broad mesopore distribution was located in the range of approximately 5–20 nm, which indicates the presence of mesopore in all FCC catalyst samples. However, the mesopore in the range of 5–20 nm was slightly reduced after catalytic reaction, suggesting that the pore loss was caused by coke formation. To the best of our knowledge, zeolite mainly contributes to microporosity for aromatization, which is the least accessible for large-size molecules. Besides that, observation and analysis of *meso-* and macropores evolution is also of great significance to understand the catalytic degradation process. The widely used techniques for porosity assessment include gas adsorption and mercury intrusion porosimetry, which provide inadequate insight into the textural properties of the catalyst over the whole range length in a three-dimensional visualization perspective.

Fig. 12 displays the calculated thickness maps of the interconnected pore networks. The volume-based thickness of each porous region is fitted with maximal spheres to calculate the pore diameter distribution [47,48]. The thickness of the fitted spheres is represented by a color map, ranging from 63 nm (blue end) to 7μ m (red end). The macro-pore size distribution(PSD) of fresh and used FCC catalysts derived from thickness map is shown in Fig. 13. The pore size of all catalysts delivered a "Gaussian" distribution. The major distribution of macropore in both fresh FCC1 and FCC2 catalysts appeared in the diameter region of 126–512 nm, with the highest frequency at around 178 nm. Compared to fresh counterparts, the spent FCC1 and FCC2 catalysts suffered a distinct reduction of large-size pores in light of color map shifting from red to blue end, suggesting a remarkable loss of porosity caused by coke formation on the surface of catalyst. Particularly, the large-size pores of more than 385 nm disappeared after catalytic reaction. As a result, the used FCC possessed much narrower PSD in the range of 136–325 nm. Some researchers elucidated that most of the reactive intermediates are easily confined in the microporous network, and the pore size of microporous zeolites is strongly related to coke formation, in spite of substantial diffusional resistance for larger hydrocarbons to access in [49,50]. The phenomenon in our study illustrated that the larger pore size also allowed a high degree of coke condensation during catalytic reaction. The similar conclusion was also discussed by Elordi et al [51]. Combined with the analysis of radial distribution in Fig. 10, it can be speculated that prior to pore blockage, coke molecules can be heterogeneously distributed not only over the zeolite crystallites, but more concentrated on *meso-* and macropores of the external surface.

The 3D skeleton model of the fresh FCC1 particle is shown in Fig. S2. The various pore size range of fresh FCC1 were distinguished, wherein the pore size less than 100 nm was marked in purple, while more than 100 nm was colored in blue. As shown in Fig S2, the small pore size

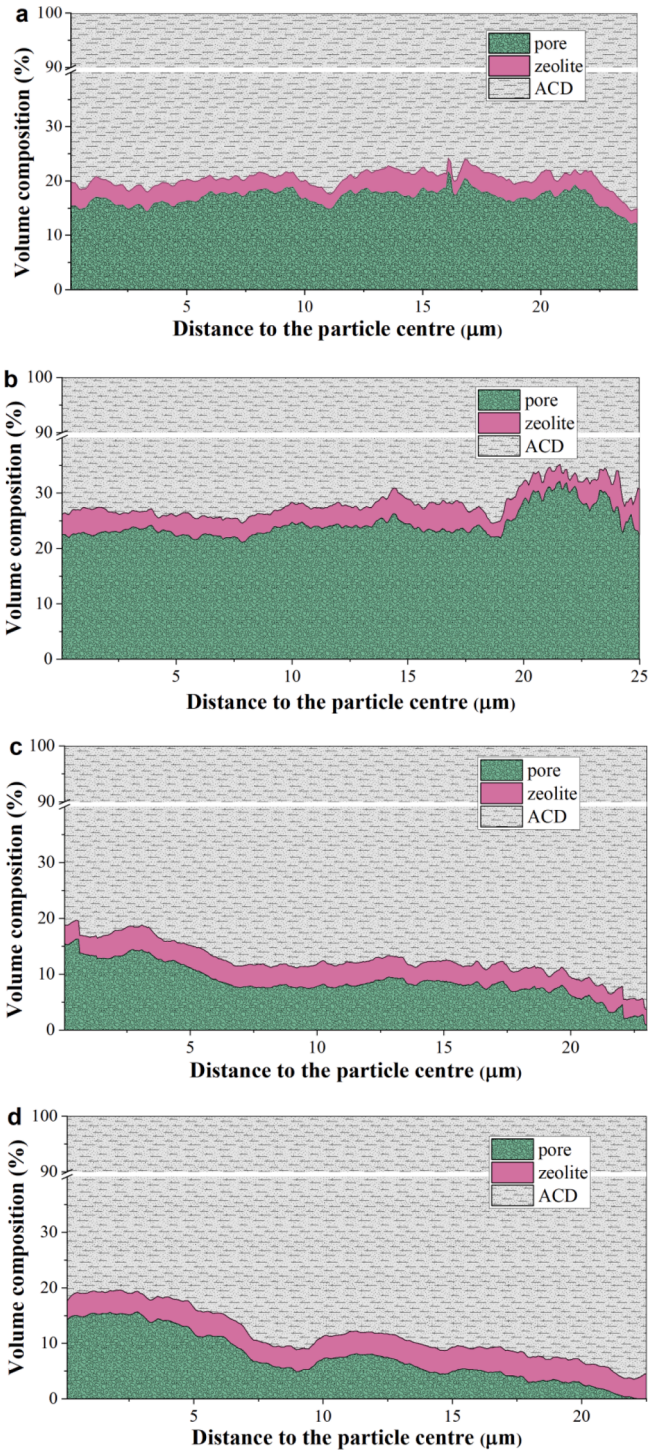

Fig. 10. Radial distribution of three-phase composition in catalyst from the core to the outermost layer of (a) fresh FCC1, (b) fresh FCC2, (c) used FCC1 and (d) used FCC2 particle.

(<100 nm) delivered an even dispersion on matrix skeleton spatially, while large pores (>100 nm) were surrounded by smaller pores and on the outer surface of catalyst. When the molten plastic polymers were cracked via random scission or end-chain scission to release initial hydrocarbon products, they would be given preference to pre-crack in the outer macropores of the matrix due to lower diffusion resistance, thus easily causing more coke formation [52]. The spatial porosity distribution of all FCC catalysts from particle center to exterior surface is shown in Fig. 14. The porosity in x-, y-, z-axis was centered around 22 % for

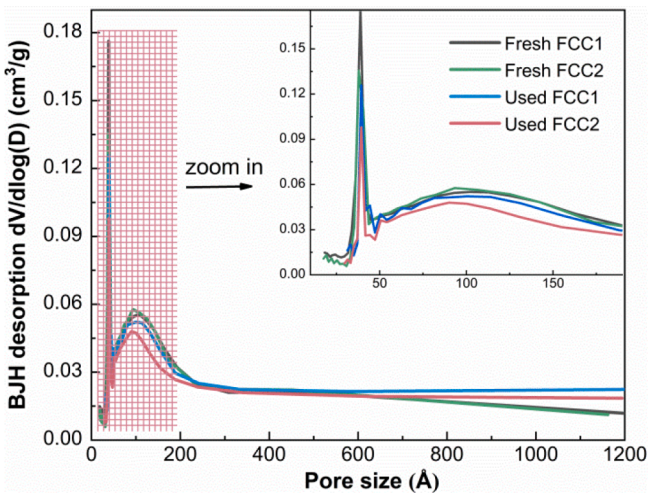

Fig. 11. Pore size distribution of fresh and used catalysts derived from N_2 desorption isotherm.

fresh FCC1 and 16 % for fresh FCC2, respectively. This implied a certain degree of pore homogeneity in FCC particle. After catalytic degradation, the porosity of catalysts decreased obviously over the whole range of length by virtues of coke formation and/or structural collapse. While the pore loss of outer surface was more serious than the internal part, indicating that the coke concentrated preferentially on the outer surface of the catalyst particles, forming the so-called external coke. The trend is in line with the result from spatial pore distribution in Fig. 10. Combined with PSD analysis, it can be concluded that macropores on the outermost surface are much easier for large compounds to attach.

In the former case, coke molecules affected the catalytic activity linearly by blocking acid site, thus changing the selectivity of reaction [53,54]. Polymer plastic (PE) contains ~80 wt% carbon of total mass in volatiles [55], which would cause considerable carbon compounds over the catalyst surface, thus deactivating catalytic activity. It is much more pronounced in the case of coke molecule blocking the access of reactants to pore channels, instead of active sites [17]. The large-size compounds are incapable to easily penetrate inside active sites due to highly diffusive mass-transport resistance, instead of giving preference to attach to macropores. The heavier coke molecules then accumulate on the outer surface and locally block the access of reactant molecules to the pore openings for isomerization, hydrogen transfer, cyclization, aromatization, or condensation.

In comparison to microporous zeolite, the external coke is of critical importance to the deactivation of zeolites in the transformation of large compounds, and an increase of opening pores on the catalyst surface improves coke tolerance and prolonged catalyst lifetime [56,57]. If this is the case, the reduction of effective pore diameter will increase the diffusion resistance of reactants in the crystallites. An important parameter related to mass transfer limitations is the accessibility of reactant molecules to the active sites located inside the catalyst particles. The higher the zeolite crystallite size, the less amount of coke is needed in order to have partial blockage of the access to zeolite pores; small crystallites present a much higher external surface area, thus limiting the effects of pore blockage. The structure of zeolite-based catalyst could be rationalized by manipulating the opening macropores and some active sites in the outermost layer of the catalyst for pre-cracking of macromolecules, and mesopores in the interior of the catalyst to reduce coke formation and diffusion resistance. The small size of zeolite crystallites is retained in the innermost structure, resulting in a larger specific surface area and more active sites.

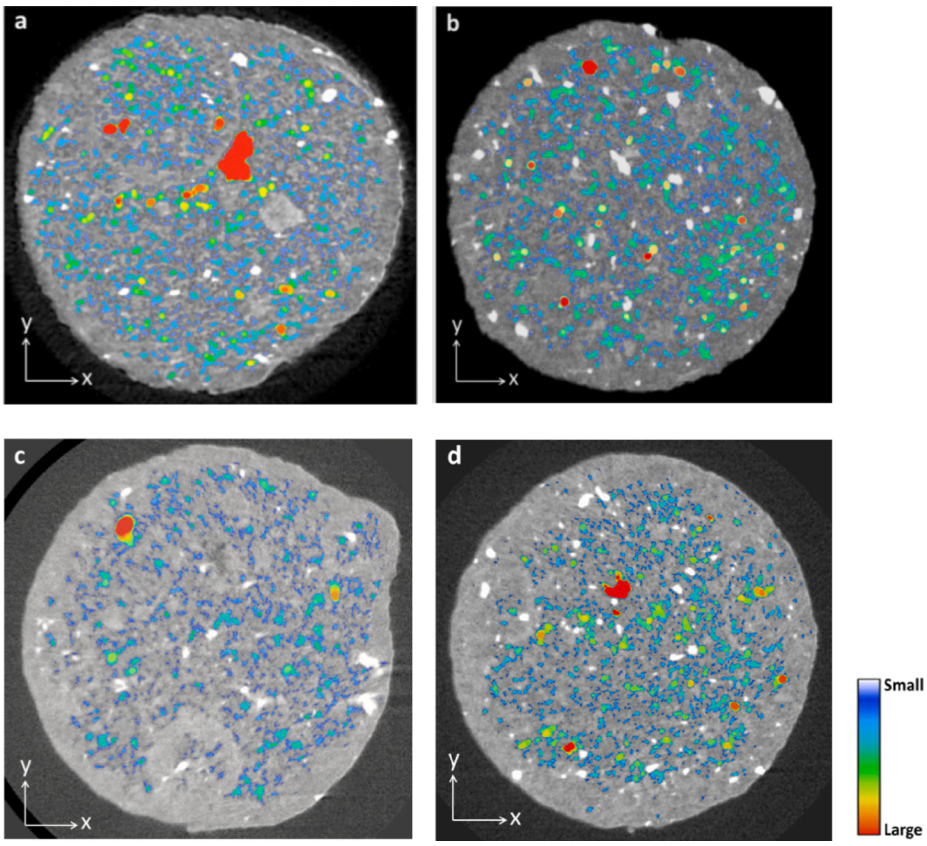

Fig. 12. The calculated thickness maps of pore networks over (a) fresh FCC1, (b) fresh FCC2, (c) used FCC1 and (d) used FCC2.

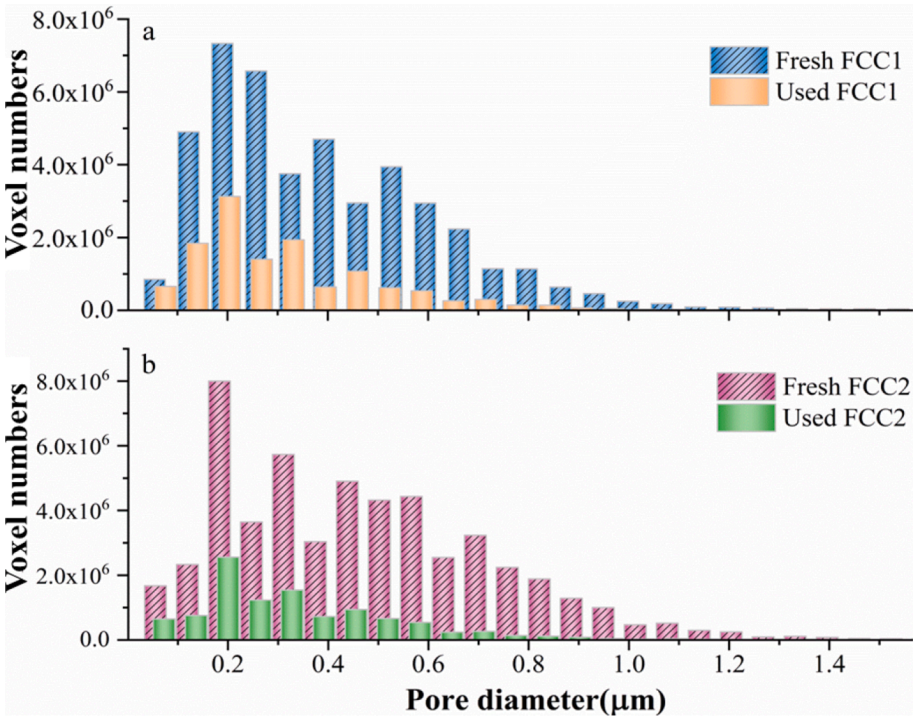

Fig. 13. The calculated macro-pore size distribution of fresh and used FCC catalyst.

4. Conclusion

In this study, *in-situ* catalytic degradation of plastic wastes to gasoline-range liquid products over FCC catalysts has been investigated in-depth. The oil and gas components over two FCC catalysts have been characterized by multiple characterizations. The structural evolution of

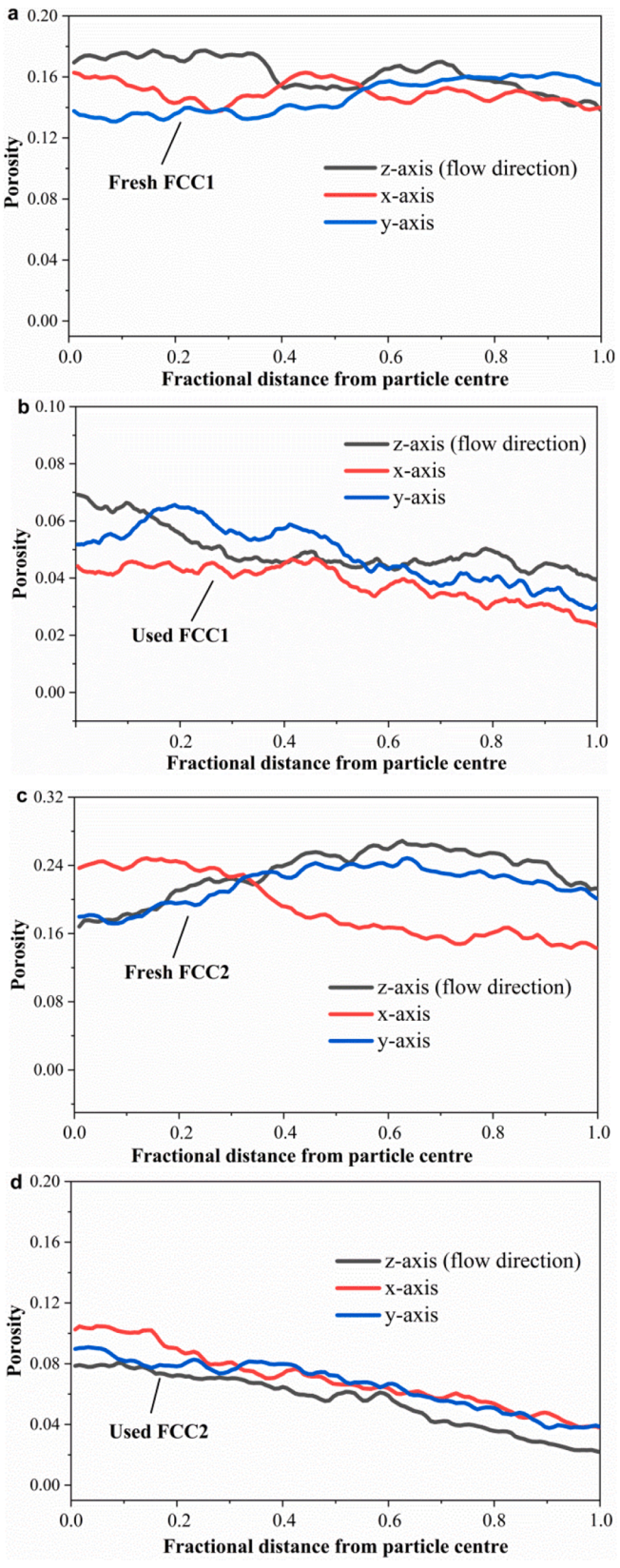

Fig. 14. The 3D porosity (in x-, y-, z-axis) of (a) fresh FCC1, (b) used FCC1, (c) fresh FCC2 and (d) used FCC2 as a function of fractional distance from particle center.

catalysts over the whole range of length scales, as well as the topology of heterogeneous pore systems with the spatial distribution of the zeolite and matrix were probed by X-ray nano-CT for insightful understanding of the degradation process. The incorporation of FCC catalysts promoted decomposition of primary liquid (C_{16}-C_{30}) to C_9-centered monocyclic aromatic species, mainly toluene, p-Xylene and various methylbenzenes. FCC1 achieved more liquid yield (51.6 %) than that (46.7 %) of FCC2. The results could be ascribed to the less surface acidity that minimized the over-cracking of secondary reaction to gas products. The analysis of X-ray nano-CT on FCCs results illustrated that fresh FCC catalysts have spatially homogeneous distribution of porosity and zeolite from the radial orientation. After catalytic reaction, the 3D porosity of FCC catalyst decreased distinctly. A large loss of pore appeared in exterior structure, while the interior pores were not significantly affected, suggesting heavy molecules derived from polymers incapable of engaging with active sites to full advantage. The above-mentioned effect is most obvious at the depth of ~16.5μ m from the outer surface of particle. The heavier coke molecules would preferably accumulated on the large pore size (>385 nm) of the external surface and locally block the access of reactant molecules to the pore openings for dehydrogenation reaction. The external coke is of critical importance to the deactivation of catalyst in the transformation of large compounds. In comparison to microporous zeolite, increasing opening pores on the catalyst surface improve coke tolerance and prolonged catalyst lifetime.

Declaration of Competing Interest

The authors declare that they have no known competing financial interests or personal relationships that could have appeared to influence the work reported in this paper.

Data availability

No data was used for the research described in the article.

Acknowledgements

The authors are grateful for financial supports provided by the Royal Society of Chemistry Enablement Grant (E21-5819318767) and Royal Society of Chemistry Mobility Grant (M19-2899), National Natural Science Foundation of China (No. 51906110), the Natural Science Foundation of Jiangsu Province, China (No. BK20190465). The authors gratefully acknowledge financial support from China Scholarship Council.

Appendix A. Supplementary data

Supplementary data to this article can be found online at https://doi.org/10.1016/j.cej.2022.138402.

References

[1] L.D. Ellis, N.A. Rorrer, K.P. Sullivan, M. Otto, J.E. McGeehan, Y. Román-Leshkov, N. Wierckx, G.T. Beckham, Chemical and biological catalysis for plastics recycling and upcycling, Nat. Catal. 4 (7) (2021) 539–556.
[2] S. Jung, S. Lee, X. Dou, E.E. Kwon, Valorization of disposable COVID-19 mask through the thermo-chemical process, Chem. Eng. J. 405 (2021) 126658.
[3] Y.S. Zhang, H.L. Zhu, D. Yao, P.T. Williams, C. Wu, D. Xu, Q. Hu, G. Manos, L. Yu, M. Zhao, P.R. Shearing, D.J.L. Brett, Thermo-chemical conversion of carbonaceous wastes for CNT and hydrogen production: a review, Sustainable Energy Fuels 5 (17) (2021) 4173–4208.
[4] G. Lopez, M. Artetxe, M. Amutio, J. Alvarez, J. Bilbao, M. Olazar, Recent advances in the gasification of waste plastics. A critical overview, Renew. Sustain. Energy Rev. 82 (2018) 576–596.
[5] J. Wang, J. Jiang, X. Meng, M. Li, X. Wang, Y. Sun, S. Pang, K. Wang, Z. Zhong, R. Ruan, A.J. Ragauskas, Promoting aromatic hydrocarbons formation via catalytic pyrolysis of polycarbonate wastes over Fe- and Ce- loaded aluminium oxide catalysts, Environ. Sci. Technol. (2020).
[6] K. Jin, P. Vozka, C. Gentilcore, G. Kilaz, N.-H. Wang, Low-pressure hydrothermal processing of mixed polyolefin wastes into clean fuels, Fuel 294 (2021) 120505.

[7] L. Wu, Y. Wang, L. Zheng, M. Shi, J. Li, Design and optimization of bio-oil co-processing with vacuum gas oil in a refinery, Energ. Convers. Manage. 195 (2019) 620–629.

[8] E. Rodríguez, A. Gutiérrez, R. Palos, F.J. Vela, M.J. Azkoiti, J.M. Arandes, J. Bilbao, Co-cracking of high-density polyethylene (HDPE) and vacuum gasoil (VGO) under refinery conditions, Chem. Eng. J. 382 (2020) 122602.

[9] Q. Wang, Y.i. Li, C. Benally, Y. Li, C. Chen, Z. An, M. Gamal El-Din, Spent fluid catalytic cracking (FCC) catalyst enhances pyrolysis of refinery waste activated sludge, J. Cleaner Prod. 295 (2021) 126382.

[10] L. Fan, P. Chen, Y. Zhang, S. Liu, Y. Liu, Y. Wang, L. Dai, R. Ruan, Fast microwave-assisted catalytic co-pyrolysis of lignin and low-density polyethylene with HZSM-5 and MgO for improved bio-oil yield and quality, Bioresour. Technol. 225 (2017) 199–205.

[11] A.S. Burange, M.B. Gawande, F.L.Y. Lam, R.V. Jayaram, R. Luque, Heterogeneously catalyzed strategies for the deconstruction of high density polyethylene: plastic waste valorisation to fuels, Green Chem. 17 (2014) 146–156.

[12] L. Fan, R. Ruan, J. Li, L. Ma, C. Wang, W. Zhou, Aromatics production from fast co-pyrolysis of lignin and waste cooking oil catalyzed by HZSM-5 zeolite, Appl. Energ. 263 (2020) 114629.

[13] K. Praveen Kumar, S. Srinivas, Catalytic co-pyrolysis of biomass and plastics (Polypropylene and Polystyrene) using spent FCC catalyst, Energy Fuels 34 (1) (2020) 460–473.

[14] Z. Sebestyén, M. Blazsó, E. Jakab, N. Miskolczi, J. Bozi, Z. Czégény, Thermo-catalytic studies on a mixture of plastic waste and biomass, J. Therm. Anal. Calorim. 147 (11) (2022) 6259–6270.

[15] E. Rodríguez, A. Gutiérrez, R. Palos, F.J. Vela, J.M. Arandes, J. Bilbao, Fuel production by cracking of polyolefins pyrolysis waxes under fluid catalytic cracking (FCC) operating conditions, Waste Manage. 93 (2019) 162–172.

[16] A. Eschenbacher, R.J. Varghese, M.S. Abbas-Abadi, K.M. Van Geem, Maximizing light olefins and aromatics as high value base chemicals via single step catalytic conversion of plastic waste, Chem. Eng. J. 428 (2022) 132087.

[17] K. Saeaung, N. Phusunti, W. Phetwarotai, S. Assabumrungrat, B. Cheirsilp, Catalytic pyrolysis of petroleum-based and biodegradable plastic waste to obtain high-value chemicals, Waste Manage. 127 (2021) 101–111.

[18] I. Vollmer, M.J.F. Jenks, R. Mayorga González, F. Meirer, B.M. Weckhuysen, Plastic waste conversion over a refinery waste catalyst, Angew. Chem. Int. Ed. 60 (29) (2021) 16101–16108.

[19] M. Qian, H. Lei, E. Villota, Y. Zhao, E. Huo, C. Wang, W. Mateo, R. Zou, Enhanced production of renewable aromatic hydrocarbons for jet-fuel from softwood biomass and plastic waste using hierarchical ZSM-5 modified with lignin-assisted re-assembly, Energ. Convers. Manage. 236 (2021) 114020.

[20] X. Lin, Z. Zhang, Q. Wang, Evaluation of zeolite catalysts on product distribution and synergy during wood-plastic composite catalytic pyrolysis, Energy 189 (2019) 116174.

[21] J. Huang, A. Veksha, W.P. Chan, A. Giannis, G. Lisak, Chemical recycling of plastic waste for sustainable material management: a prospective review on catalysts and processes, Renew. Sustain. Energy Rev. 154 (2022) 111866.

[22] P.A.K.B. Sibao Liu, Plastic waste to fuels by hydrocracking at mild conditions, Sci. Adv. (2021).

[23] J. Wang, J. Jiang, X. Wang, R. Wang, K. Wang, S. Pang, Z. Zhong, Y. Sun, R. Ruan, A.J. Ragauskas, Converting polycarbonate and polystyrene plastic wastes intoaromatic hydrocarbons via catalytic fast co-pyrolysis, J. Hazard. Mater. 386 (2020) 121970.

[24] Y.-K. Park, J.S. Jung, J. Jae, S.B. Hong, A. Watanabe, Y.-M. Kim, Catalytic fast pyrolysis of wood plastic composite over microporous zeolites, Chem. Eng. J. 377 (2019) 119742.

[25] P. Lettieri, D. Newton, J.G. Yates, Homogeneous bed expansion of FCC catalysts, influence of temperature on the parameters of the Richardson-Zaki equation, Powder Technol. 123 (2-3) (2002) 221–231.

[26] D. Xu, Y. Xiong, J. Ye, Y. Su, Q. Dong, S. Zhang, Performances of syngas production and deposited coke regulation during co-gasification of biomass and plastic wastes over Ni/γ-Al2O3 catalyst: Role of biomass to plastic ratio in feedstock, Chem. Eng. J. 392 (2020), 123728.

[27] Y.S. Zhang, X. Lu, R.E. Owen, G. Manos, R. Xu, F.R. Wang, W.C. Maskell, P. R. Shearing, D.J.L. Brett, Fine structural changes of fluid catalytic catalysts and characterization of coke formed resulting from heavy oil devolatilization, Appl. Catal. B 263 (2020), 118329.

[28] J. Schindelin, I. Arganda-Carreras, E. Frise, V. Kaynig, M. Longair, T. Pietzsch, S. Preibisch, C. Rueden, S. Saalfeld, B. Schmid, J. Tinevez, D.J. White, V. Hartenstein, K. Eliceiri, P. Tomancak, A. Cardona, Fiji: an open-source platform for biological-image analysis, Nat. Methods 9 (2012) 676–682.

[29] M. Thommes, Physical adsorption characterization of nanoporous materials, Chem.-Ing.-Tech. 82 (7) (2010) 1059–1073.

[30] C.F. Toncón-Leal, J. Villarroel-Rocha, M.T.P. Silva, T.P. Braga, K. Sapag, Characterization of mesoporous region by the scanning of the hysteresis loop in adsorption-desorption isotherms, Adsorption 27 (7) (2021) 1109–1122.

[31] T. Zelenka, Adsorption and desorption of nitrogen at 77 K on micro- and meso-porous materials: study of transport kinetics, Micropor. Mesopor. Mat. 227 (2016) 202–209.

[32] P.I. Ravikovitch, A.V. Neimark, Characterization of nanoporous materials from adsorption and desorption isotherms, Colloids Surf., A 187–188 (2001) 11–21.

[33] G. Fadillah, I. Fatimah, I. Sahroni, M.M. Musawwa, T.M.I. Mahlia, O. Muraza, Recent progress in low-cost catalysts for pyrolysis of plastic waste to fuels, Catalysts 11 (2021) 837.

[34] D.K. Ratnasari, M.A. Nahil, P.T. Williams, Catalytic pyrolysis of waste plastics using staged catalysis for production of gasoline range hydrocarbon oils, J. Anal. Appl. Pyrol. 124 (2017) 631–637.

[35] D. Yao, H. Yang, H. Chen, P.T. Williams, Investigation of nickel-impregnated zeolite catalysts for hydrogen/syngas production from the catalytic reforming of waste polyethylene, Appl. Catal. B 227 (2018) 477–487.

[36] J.A. Onwudili, C. Muhammad, P.T. Williams, Influence of catalyst bed temperature and properties of zeolite catalysts on pyrolysis-catalysis of a simulated mixed plastics sample for the production of upgraded fuels and chemicals, J. Energy Inst. 92 (5) (2019) 1337–1347.

[37] A. López, I. de Marco, B.M. Caballero, M.F. Laresgoiti, A. Adrados, A. Aranzabal, Catalytic pyrolysis of plastic wastes with two different types of catalysts: ZSM-5 zeolite and Red Mud, Appl. Catal. B 104 (3-4) (2011) 211–219.

[38] A. Tennakoon, X. Wu, A.L. Paterson, S. Patnaik, Y. Pei, A.M. LaPointe, S.C. Ammal, R.A. Hackler, A. Heyden, I.I. Slowing, G.W. Coates, M. Delferro, B. Peters, W. Huang, A.D. Sadow, F.A. Perras, Catalytic upcycling of high-density polyethylene via a processive mechanism, Nature, Catalysis 3 (11) (2020) 893–901.

[39] C. Engtrakul, C. Mukarakate, A.K. Starace, K.A. Magrini, A.K. Rogers, M.M. Yung, Effect of ZSM-5 acidity on aromatic product selectivity during upgrading of pine pyrolysis vapors, Catal. Today 269 (2016) 175–181.

[40] F. Krumeich, J. Ihli, Y. Shu, W.-C. Cheng, J.A. van Bokhoven, Structural changes in deactivated fluid catalytic cracking catalysts determined by electron microscopy, ACS Catal. 8 (5) (2018) 4591–4599.

[41] C. Prehal, S. Grätz, B. Krüner, M. Thommes, L. Borchardt, V. Presser, O. Paris, Comparing pore structure models of nanoporous carbons obtained from small angle X-ray scattering and gas adsorption, Carbon 152 (2019) 416–423.

[42] B. Kayaalp, S. Lee, K. Klauke, J. Seo, L. Nodari, A. Kornowski, W. Jung, S. Mascotto, Template-free mesoporous $La_{0.3}Sr_{0.7}Ti_1$-x$Fe_xO_{3\pm}$ for CH_4 and CO oxidation catalysis, Appl. Catal. B: Environ. 245 (2019) 536–545.

[43] U. Khalil, Z. Liu, C. Peng, N. Hikichi, T. Wakihara, J. García-Martínez, T. Okubo, S. Bhattacharya, Ultrafast surfactant-templating of *BEA zeolite: an efficient catalyst for the cracking of polyethylene pyrolysis vapours, Chem. Eng. J. 412 (2021), 128566.

[44] D. Xu, S. Yang, Y. Su, Y. Xiong, S. Zhang, Catalytic conversion of plastic wastes using cost-effective bauxite residue as catalyst into H_2-rich syngas and magnetic nanocomposites for chrome(VI) detoxification, J. Hazard. Mater. 413 (2021) 125289.

[45] J.C. Groen, L.A.A. Peffer, J. Pérez-Ramírez, Pore size determination in modified micro- and mesoporous materials. Pitfalls and limitations in gas adsorption data analysis, Microporous Mesoporous Mater. 60 (1-3) (2003) 1–17.

[46] P. Pang, H. Han, L. Hu, C. Guo, Y. Gao, Y. Xie, The calculations of pore structure parameters from gas adsorption experiments of shales: which models are better? J. Nat. Gas Sci. Eng. 94 (2021) 104060.

[47] T. Hildebrand, P. Ruegsgger, A new method for the model-independent assessment of thickness in three-dimensional images, J. Microsc-Oxford 185 (1997) 65–75.

[48] J. Ihli, R.R. Jacob, M. Holler, M. Guizar-Sicairos, A. Diaz, J.C. da Silva, D. Ferreira Sanchez, F. Krumeich, D. Grolimund, M. Taddei, W.-C. Cheng, Y. Shu, A. Menzel, J. A. van Bokhoven, A three-dimensional view of structural changes caused by deactivation of fluid catalytic cracking catalysts, Nat. Commun. 8 (1) (2017).

[49] X. Xu, Y. Zhang, X. Li, X. Xia, H. Jiang, A. Toghan, Comparative study on the catalytic behaviors of zeolites with different diffusion limitation in ethane aromatization, Micropor. Mesopor. Mat. 315 (2021) 110926.

[50] X.u. Hou, L. Zhao, Z. Diao, Roles of alkenes and coke formation in the deactivation of ZSM-5 zeolites during n-pentane catalytic cracking, Catal. Lett. 150 (9) (2020) 2716–2725.

[51] G. Elordi, M. Olazar, G. Lopez, P. Castaño, J. Bilbao, Role of pore structure in the deactivation of zeolites (HZSM-5, H β and HY) by coke in the pyrolysis of polyethylene in a conical spouted bed reactor, Appl. Catal. B 102 (2011) 224–231.

[52] E.T. Vogt, B.M. Weckhuysen, Fluid catalytic cracking: recent developments on the grand old lady of zeolite catalysis, Chem. Soc. Rev. 44 (2015) 7342–7370.

[53] J. Liang, G. Shan, Y. Sun, Catalytic fast pyrolysis of lignocellulosic biomass: critical role of zeolite catalysts, Renew. Sustain. Energy Rev. 139 (2021) 110707.

[54] I. Hita, T. Cordero-Lanzac, F.J. García-Mateos, M.J. Azkoiti, J. Rodríguez-Mirasol, T. Cordero, J. Bilbao, Enhanced production of phenolics and aromatics from raw bio-oil using HZSM-5 zeolite additives for PtPd/C and NiW/C catalysts, Appl. Catal. B 259 (2019), 118112.

[55] A. Arregi, M. Amutio, G. Lopez, M. Artetxe, J. Alvarez, J. Bilbao, M. Olazar, Hydrogen-rich gas production by continuous pyrolysis and in-line catalytic reforming of pine wood waste and HDPE mixtures, Energ. Convers. Manage. 136 (2017) 192–201.

[56] L. Lakiss, F. Ngoye, C. Canaff, S. Laforge, Y. Pouilloux, Z. Qin, M. Tarighi, K. Thomas, V. Valtchev, A. Vicente, L. Pinard, J. Gilson, C. Fernandez, On the remarkable resistance to coke formation of nanometer-sized and hierarchical MFI zeolites during ethanol to hydrocarbons transformation, J. Catal. 328 (2015) 165–172.

[57] G. Dai, S. Wang, Q. Zou, S. Huang, Improvement of aromatics production from catalytic pyrolysis of cellulose over metal-modified hierarchical HZSM-5, Fuel Process. Technol. 179 (2018) 319–323.